CHAPTER 3

Heteroatom Effect on Photophysical Properties of 2-(2'-Hydroxyphenyl)benzimidazole and Its Derivatives as Fluorescent Dyes: a TD-DFT Study

3.1 Introduction

Intramolecular hydrogen bonding can be considered an important feature in some organic dyes due to its wide range of applications including antibiotic agents [109, 110], laser dyes [41], plastic scintillation [111], optical materials and fluorescent probes [43]. The last has particularly become an active application that can be applied in chemical and biological systems [112]. Generally, fluorescent probes in biological systems require highly sensitive and specific binding to analytes in cells [113]. Desirable characters for probing in cells and tissue samples include long wavelengths (preferrably in red or near-infrared region) and high fluorescence intensities [114]. Past publications on successful organic fluorescent probes have reported the derivatives of fluorescein [24], rhodamine [9, 115], coumarin [11, 12], boron-dipyrromethene (BODIPY) [13, 14] and cyanine [116].

Beside the mentioned dyes, molecules undergoing excited-state intramolecular proton transfer (ESIPT) have emerged as new and effective fluorescent probes due to their large Stoke's shifts compared to their non-ESIPT counterparts [117]. ESIPT compounds with relatively simple structures, such as 2-(2'-Hydroxyphenyl)benzimidazole (HBI), 2-(2'-Hydroxyphenyl)benzoxazole (HBO) and 2-(2'-Hydroxyphenyl)benzothiazole (HBT), are frequently studied on there photophysical properties due to their less complexity in syntheses and high yields of ESIPT [64]. General proton transfer photocycle of HBX (general term for HBI, HBO and HBT) is shown in Scheme 1. The ESIPT of HBI [118-120], HBO [119, 121-124] and HBT [125-127] and their derivatives has attracted much attention because of their application uses

in laser dyes [128], photostabilizers [128, 129], chemical sensors [59, 130], molecular switches [131], light-emitting diode devices [128, 132] and fluorescent probes in biological systems [112, 128, 133].

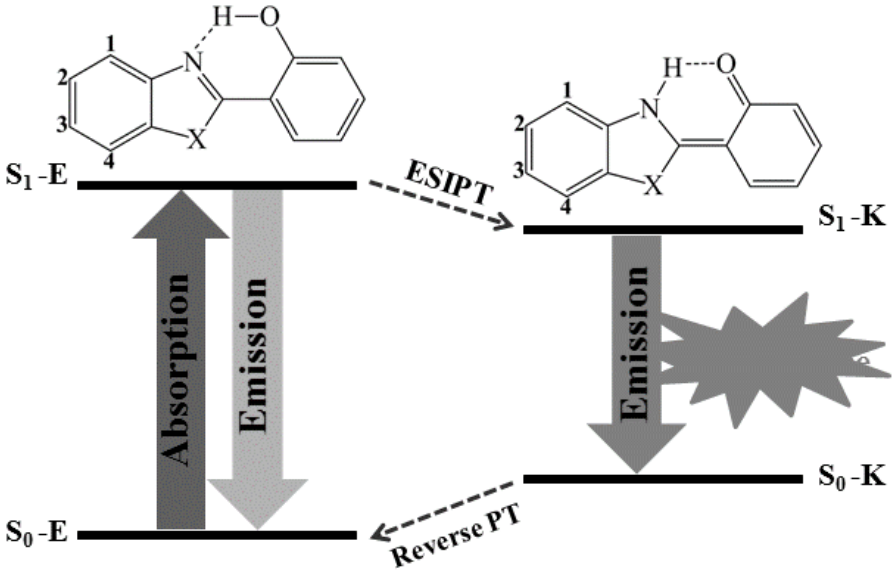

Figure 3.1 Excited-state intramolecular proton transfer (ESIPT) of the HBX molecules (where X = NH, O and S, respectively). S_0 is the ground state and S_1 is the first lowest excited-state. E is enol form and K is keto form.

ESIPT of HBX is strongly influenced by the nature of the substituents and their attachment positions as indicated by several combined experimental and theoretical studies. Two investigations by Oshima [134] and Seo [135] reported photophysical behaviors of HBO derivatives having -OMe and -NEt_2 groups as electron donating groups (EDG) on 7-position and electron withdrawing groups (EWG) such as -CHO and -COOEt groups on 3-position of HBO (see Fig. 1). The enol absorption spectra of substituted derivatives are red-shifted compared to that of HBO because the effects of either EDG or EWG decrease HOMO-LUMO energy gaps of substituted derivatives. Meanwhile, the keto emission of HBO derivatives having EDG exhibited blue shifts because of the lowering of HOMO energy levels by inductive effects of EDG, but the keto emission spectra of the HBO derivatives having EWG at 3-position were red-shifted due to the contribution of π-conjugated delocalization extended on benzoxazole ring.

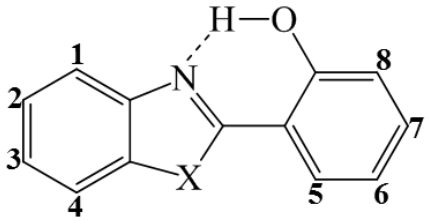

Figure 3.2 Molecular structures of HBX derivatives, where X = NH, O and S namely 2-(2'-Hydroxyphenyl)benzimidazole (HBI), 2-(2'-Hydroxyphenyl)benzoxazole (HBO) and 2-(2'-Hydroxyphenyl)benzothiazole (HBT), respectively. Numbers 1-8 represent the substitution position by substituents and hetero nitrogen atoms.

For HBT derivatives, the photophysical effects of substituents in benzothiazole ring have been reported by Wang et al. [128] and Kim et al. [135]. Both EDG (–CH_3, –OCH_3 and –OH) and EWG (–F, –Br, –CF_3 and –COOH) in 3-position of HBT were chosen. Their results indicated that both enol absorption and keto emission spectra of these derivatives move to longer wavelengths when the power of electron donating effect of the substituent increases, leading to decrease of the HOMO-LUMO energy gaps (both EDG and EWG strongly increased the HOMO more than the LUMO energy levels) [136].

For HBI derivatives, the effects of EDG (–OH, –CH3, –$NHCOCH_3$, –NH_2, –$N(CH_3)_2$) substituted at 5-position, (–OH, –OCH_3) at 6-position and EWG (–F, –Cl) substituted at 6-position of HBI on photophysical properties were investigated by Akutzu et al. [130]. Furthermore, Chipem et al. [129, 137] studied HBI derivatives, which can be generated by the substitution of aromatic carbon atoms by nitrogen atom in 2-, 4- and 2,4- positions of benzimidazole ring. The hetero nitrogen substitution in 4- and 2,4- positions of benzimidazole ring affects the enol absorption and keto emission with red shift. But the enol absorption and keto emission of 2-position substituted gives blue shift compared to those of HBI. Moreover, they reported the substitution of carbon atom by nitrogen atom in 5-, 6-, 7-, 8- and 5,7-position in phenyl moiety. Both enol absorption and keto emission of all derivatives are red shift except the 7-position substitution which gives blue shifts [129]. The red-shifted spectra suggest that the lone pair of electron in the substituted hetero nitrogen is involved in π-conjugation which might help lower the HOMO-LUMO energy gap.

In addition to the above studies, sole computational studies have also been carried out. Although limited in the accuracy, they are still useful in the compound screening and also give further information that had not been accessed by experiments. Recently in separated works, Irgibaeva et al.[138] and Dangngern et al.[132] studied photophysical properties of HBO derivatives having EDG (–CH_3, –OCH_3) or EWG (–CN, –CHO, –$COOC_2H_5$, –NO_2) on the 3- and 7-position. Both enol absorption and keto emission spectra of all derivatives are red-shifted compared to those of HBO because the influence of EWG substituents increases the stability of π-conjugation. In 2014, Padalklar et al. [139], investigated the ESIPT of HBO derivatives with NH_2 as electron donor and NO_2 as electron acceptor at 2- and 3- position of benzoxazole ring. The effect of NO_2 (electron acceptor) increases the acidity of proton donor and basicity of proton acceptor and favors the ESIPT process, resulting in the dual emission spectra of HBO derivatives. While, the NH_2 (electron donor) decreases the basic nature of HBO derivatives and hinders the ESIPT process. Lately in 2016, the theoretical study of substituted HBI derivatives has been reported by Jacquemin et al. [140] They calculated the enol and keto emission spectra of HBI derivatives, which substituted by EDG (–NMe_2, –NH_2, –OCH_3) and EWG (–CN, –CH_3, –F) in various positions (2-, 3-, 6- and 7-) of HBI. Most of their keto emission spectra give red shift relative to that of HBI because the strong geometrical reorganization following absorption. In addition, they predicted stabilization of enol (E^*) and keto (K^*) forms at the S_1 using relative activation energy of substituted molecules (compared to activation energy of non-substituted molecule). The effect of substituents helps stabilizing K^* more than E^* and hence to thermodynamically favor the ESIPT process. From all previous studies on HBX derivatives as mentioned above, it hinted that the effect of substituents and hetero nitrogen atom substitution on spectral characteristics of HBX derivatives play an important role for the photophysical properties. In addition, the substitution in HBX derivatives influences the ESIPT efficiency because they adjust the strength of hydrogen bond (lengthen O–H bond and shorten intramolecular N–H bond) [128, 137].

Computational chemistry has nowadays become an effective tool for screening the candidates before real synthesis can be effectively used. The obtained information particular on photophysical properties of new designed fluorescent dyes will be very useful as guidance for chemists who are interested in developing the novel and effective

ESIPT fluorescent dyes. The merits of these studies are helpful to the research on the modification of the HBX derivatives for the desired properties by saving costs and environmental hazards resulting from synthesizing unnecessary compounds for the test [141-143]. The obtained information particular on photophysical properties of new designed fluorescent dyes will be very useful as guidance for chemists who are interested in developing the novel and effective ESIPT fluorescent dyes.

The goal of this work is to understand the effect of heteroatom substitution on spectral characteristics of HBX derivatives. Absorption and emission spectra of HBX derivatives were analyzed to study the photophysical property and Stokes shift of these derivatives. The strength of hydrogen bond of HBX derivatives are investigated both in S_0 and S_1. In addition, the chances of ESIPT occurrence were studied by potential energy curves (PECs). Proton transfer (PT) coordinates both in S_0 and S_1 were scanned to obtain the barrier energy. The lowest barrier energy from PECs results will show which the ESIPT could occur and will be compared the available data.

3.2 Computational Details

The ground-state optimizations and vibrational frequencies of HBI were performed in solution phase using density functional theory (DFT) method with seven different exchange-correlation functionals, which consist of four hybrid functionals (B3LYP [95], PBE0 [99], M06, and M062X [100]) and three long-range corrected hybrid functionals; ωB97XD[144], CAM-B3LYP [102], LC-BLYP [145]) with 6-311+G(d,p) basis set. The brief details of each functional are as follows: the hybrid B3LYP and PBE0 functionals include 20% and 25% of Hartree-Fock (HF) exchange, respectively. The M06 and M062X are the hybrid functional of Truhlar and Zhao [100].Three long-range corrected hybrid functionals include ωB97XD, CAM-B3LYP and LC-BLYP, which are Head-Gordon, Handy and Hirao methods, respectively. The optimizations in the solution phase taking effect of water into account through dielectric constant were performed by using SCRF method through the non-equilibrium polarizable continuum model calculations (C-PCM) framework to confirm the consistency with available data [146]. The global minimum of all S_0 geometries was confirmed by no imaginary frequency.

The suitable method from the various choice for predicting the enol absorption spectra of HBI is B3LYP with 6-311+G(d,p) basis set in solution phase, in which the variations of all functionals compared to experimental data were discussed in section 3.3.1. The molecular structures of all derivatives shown in Figure 3.3 will be used to perform the vertical excitation energy for absorption spectra. S_1 optimization and absorption spectra of selected molecules were performed using time-dependent B3LYP (TD-B3LYP) with same basis set.

The selected molecules with more red-shifted and large Stokes shift will be further investigated for the chances of ESIPT. S_0 and S_1 PESs of selected molecules were also scanned by constrained optimization by fixing O–H bond length at a series of values to find the barrier height [147, 148]. Furthermore, the strength of hydrogen bond of selected derivatives was investigated by using the calculated infrared spectra of the O–H bonds in S_0 and S_1. All calculations were carried out using Gaussian 09 program [149].

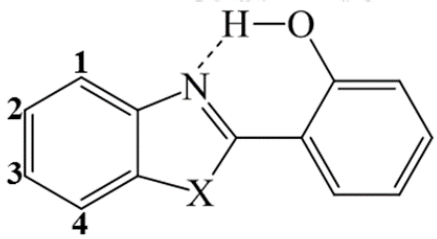

Position of N atom	X = NH	X = O	X = S
-	HBI	HBO	HBT
1	HBI1	HBO1	HBT1
2	HBI2	HBO2	HBT2
3	HBI3	HBO3	HBT3
4	HBI4	HBO4	HBT4
1,2	HBI12	HBO12	HBT12
1,3	HBI13	HBO13	HBT13
1,4	HBI14	HBO14	HBT14
2,3	HBI23	HBO23	HBT23
2,4	HBI24	HBO24	HBT24
3,4	HBI34	HBO34	HBT34

Figure 3.3 Molecular structures of HBX molecules. 1, 2, 3 and 4 indicate the substitution positions by hetero nitrogen atom used in this work.

3.3 Results and Discussion

3.3.1 The Effect of DFT Functionals

Suitable methods of DFT and TD-DFT are very important to describe the spectral characteristics of HBI derivatives. Various functionals were carried out to obtain S_0 equilibrium structures and to reveal the functional influence on the absorption wavelength of HBI molecule. The calculated maximum wavelengths of HBI from all functionals are listed in Table 3.1 to compare with the experimental value. The calculated absorption spectra of HBI by various methods were plotted in Figure 3.4.

The maximum wavelengths from the TD-B3LYP and TD-PBE0 hybrid functionals are 316 nm and 307 nm, respectively, which are in good agreement with experimental data at 312.5 nm [146]. These two functions show slight shift of absorption peaks from the experimental value with the deviation of 3.5 nm and 5.5 nm for the TD-B3LYP and TD-PBE0, respectively. Therefore, the TD-B3LYP and TD-PBE0 hybrid functions can efficiently characterize spectral properties of HBI. While other hybrid functionals (TD-M06 and TD-M062X) tend to greatly overestimate excitation energies. The deviations between the calculated and experimental wavelength ($\Delta\lambda$) are 37.5 nm for TD-M06 and 27.5 nm for TD-M062X functionals. For long-range corrected hybrid functionals, all three of them fail to reproduce the the maximum wavelength of HBI compared to experimental data because these functionals provide large deviation between the calculated and experimental wavelengths. The deviations between the calculated and experimental wavelengths by using TD-ωB97XD, TD-CAM-B3LYP and TD-LC-BLYP methods are 26.5, 25.5 and 46.5 nm, respectively.

Consequently, both TD-B3LYP and TD-PBE0 hybrid functionals can be further used to obtain the spectral characteristics of HBI derivatives, and the obtained information from these two functionals would be equally useful. However, based on our results, the TD-B3LYP functional gives better-calculated results compared to experimental data. Therefore, we use B3LYP to further investigate other electronic properties of HBX derivatives. In addition, TD-B3LYP has been found to be the suitable method and employed in our previous work [132] to investigate the photophysical properties of HBO derivatives.

Table 3.1 Maximum wavelength (λ_{max}) of first excitation and deviation between the calculated and experimental wavelengths ($\Delta\lambda$) for HBI calculated by various TD-DFT methods with 6-311+G(d,p) basis set.

Methods	λ_{max} (nm)	$\Delta\lambda$ (nm)
Expt.[a]	313	0.0
TD-B3LYP	316	3.5
TD-PBE0	307	5.5
TD-M06	275	37.5
TD-M062X	285	27.5
TD-ωB97XD	286	26.5
TD-CAM-B3LYP	287	25.5
TD-LC-BLYP	266	46.5

[a] The experimental data is reported in Ref.[146]

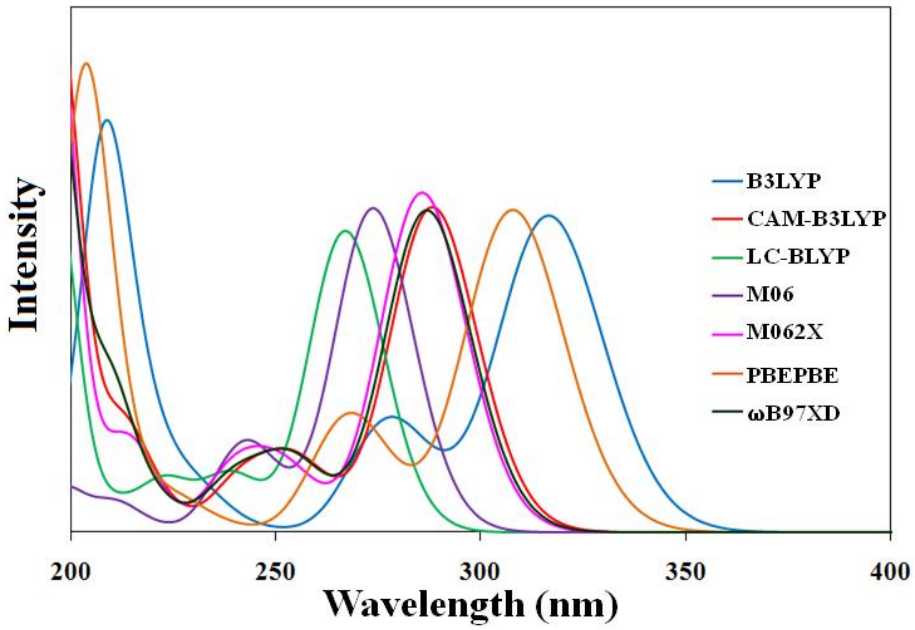

Figure 3.4 Calculated absorption spectra of HBI by various TD-DFT methods with hybrid exchange functional at 6-311+G(d,p) basis set.

3.3.2 Ground State Optimization and Structural Parameter of HBX Derivatives

All derivatives were optimized with suitable DFT functional at B3LYP/6-311+G(d,p) basis set in water. Structural parameters of HBX derivatives in term of selected bond lengths and dihedral angles are listed in Table 3.2. The bond lengths of C–C bond of HBI and HBO derivatives are 1.45 Å, while those of HBT derivatives are in the range of 1.43-1.46 Å. The selected bond lengths of O–H bond of all derivatives are 0.99 Å. Dihedral angles between ring of benzimidazole and hydroxyphenyl are found to planar for HBI, HBO and HBT derivatives. Therefore, adding heteroatoms or nitrogen atom in HBX derivatives does not affect the planarity of these derivatives.

Table 3.2 The selected bond lengths (Å) and dihedral angles (degree) for ground state optimized structures calculated by B3LYP/6-311+G(d,p) level of theory.

Code	NCCC	C–C	O–H	Code	NCCC	C–C	O–H	Code	NCCC	C–C	O–H
HBI	0.08	1.45	0.99	**HBO**	0.00	1.45	0.99	**HBT**	0.01	1.45	0.99
HBI1	0.00	1.45	0.99	**HBO1**	0.00	1.45	0.99	**HBT1**	0.04	1.45	0.99
HBI2	0.00	1.45	0.99	**HBO2**	0.00	1.45	0.99	**HBT2**	0.01	1.45	0.99
HBI3	0.01	1.45	0.99	**HBO3**	0.00	1.45	0.99	**HBT3**	0.03	1.45	0.99
HBI4	0.01	1.45	0.99	**HBO4**	0.00	1.45	0.99	**HBT4**	0.07	1.45	0.99
HBI12	0.02	1.45	0.99	**HBO12**	0.00	1.45	0.99	**HBT12**	0.00	1.45	0.99
HBI13	0.33	1.45	0.99	**HBO13**	0.09	1.45	0.99	**HBT13**	0.00	1.43	0.99
HBI14	0.19	1.45	0.99	**HBO14**	0.02	1.45	0.99	**HBT14**	0.04	1.45	0.99
HBI23	0.01	1.45	0.99	**HBO23**	0.01	1.45	0.99	**HBT23**	0.02	1.45	0.99
HBI24	0.01	1.45	0.99	**HBO24**	0.02	1.45	0.99	**HBT24**	0.01	1.46	0.99
HBI34	0.02	1.45	0.99	**HBO34**	0.04	1.45	0.99	**HBT34**	0.01	1.45	0.99

3.3.3 Calculated Absorption Spectra of HBX Derivatives

In this section, we investigate the absorption spectra of HBX derivatives and the effect of hetero nitrogen atom substitution. The calculated maximum wavelength of absorption spectra of enol form (λ_{max}), excitation energies, oscillator strengths (*f*) and major contributions of HBX derivatives are listed in Table 3.3 and the calculated absorption spectra of HBX derivatives are shown in Figure 3.5.

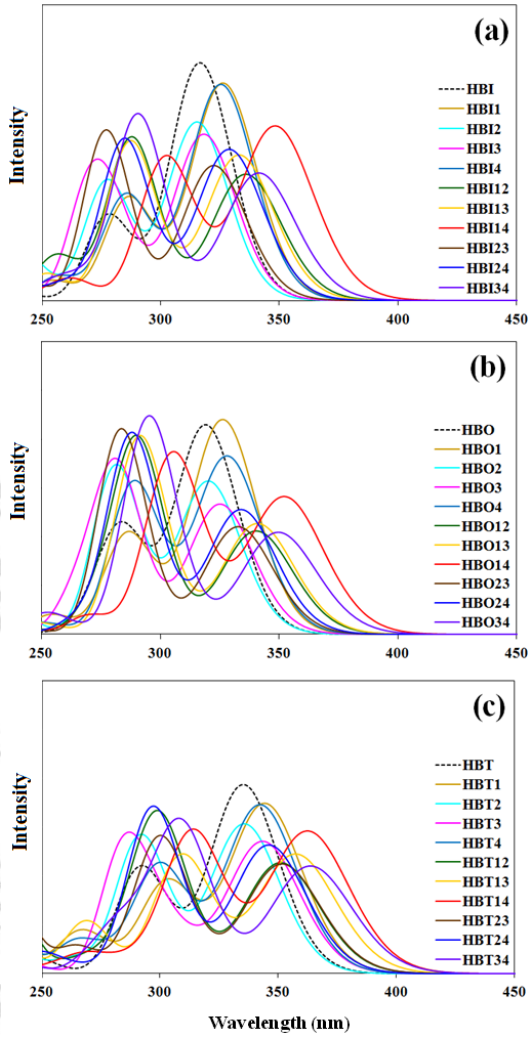

Figure 3.5 Calculated absorption spectra of (a) HBI, (b) HBO, (c) HBT and their derivatives in water. The calculations were performed using TD-B3LYP/6-311+G(d,p) level.

From the maximum absorption wavelengths, it can be observed that mono substitution of hetero nitrogen in benzene ring resulted in the promotion of red shift. The red shift is even pronounced upon the introduction of the second nitrogen heteroatoms. The degree of influence of the heteroatom substitutions is in the order of HBT > HBO > HBI. Furthermore, when considering the position of substitution, the substitution at 1- and 4- position gives stronger red shift compared to other positions. The combination of the disubstitution at both 1- and 4-positions, as expected, gives the largest red shift in all three parent compounds compared to others.

In HBI derivatives, the least affected by the heteroatom substitution, the monosubstitution of HBI resulted in slight differences in the absorption spectra. The strongest effect can be observed in the compound HBI1 and HBI4 with λ_{max} of 325 and 326 nm, respectively. The disubstituted compounds further enhance the red shift, where the strongest enhancement is the 1,4-disubstituted derivatives giving the λ_{max} as long as 348 nm. In the case of HBO derivatives, the λ_{max} of all HBO derivatives are red-shifted compared to that of HBO (λ_{max}= 318nm). Monosubstitution causes the more noticeable red shift in HBO compared to HBI. The λ_{max} of monosubstituted derivatives ranges from 320 to 327 nm. As expected, the disubstitution intrigues larger red shift ranging from 333 to 351 nm. The calculated absorption spectra of enol forms of HBO14 and HBT34 are 351 nm and 349 nm, respectively, which are more red shift than other derivatives. In HBI derivatives, photophysical properties of HBT is affected by the hetero nitrogen substitution similar to that of HBO. However, the absorption wavelength of the parent compound is already longer than HBO and HBI, the spectra of the substituted derivatives appear even closer to the visible region. In monosubstituted derivatives, their absorption peaks are predicted to be in the range of 335-344 nm. Disubstitution of hetero nitrogen atoms moves the absorption peaks to the range of 350-362 nm. Similarly, the furthest red shift compounds are HBT14 and HBT34, which have the calculated maximum wavelengths of 362 nm and 363 nm, respectively.

Based on our calculated absorption spectra of all HBX derivatives, the results indicate that an introducing of hetero nitrogen atom into the benzene ring of HBX increases λ_{max} of HBI derivatives. The red shift imply that the lone pair of electron in the substituted hetero nitrogen has the effect on the π-conjugated system of benzimidazole ring (HBI), benzoxazole ring (HBO) and benzothiazole ring (HBT), where the nitrogen atoms are placed at 1,4 or 3,4 positions. Lone pair electron of substituted hetero nitrogen might stabilize the conjugate system in benzene ring of HBX derivatives, causing the lowering lowest unoccupied molecular orbital (LUMO) or the elevating highest occupied molecular orbital (HOMO) or both. As a consequence the red-shifted spectra of HBX derivatives with substituted hetero nitrogen could be observed [129]. The explanation on effect of adding heteroatom into HBX parent

molecules in terms of frontier molecular orbitals and HOMO-LUMO gaps will be given in section 3.3.4.

3.3.4 Frontier Molecular Orbitals and Energy Band Gap of HBX Derivatives

Frontier molecular orbitals of selected HBX derivatives (hetero nitrogen atoms substituted at 1,4 and 3,4 positions) are illustrated in Figure 3.6 and those of other HBX derivatives are shown in Figure 3.7-3.9. The main contributions of electronic transition of all derivatives have similar characters. The electron density contributions of HBI and its derivatives are in the range of 94-97% (HOMO→LUMO). The electron density contributions of HBO and HBT derivatives are in the range of 95-97% and 96-97%, respectively. From the frontier molecular orbitals of HBX derivatives, the decrease of electron density in the hydroxyl group and increase in heteroatom are expected to directly influence the intramolecular hydrogen bonding strength, in which the bond lengths of N–H are shortened upon excitation to S_1 (see Table S1 of the Supplementary material). The strength of hydrogen bonding affected by the substitution of nitrogen heteroatoms into benzene ring of HBX will be explained in the Section 3.3.7. In addition to frontier molecular orbitals, the change of electron density upon absorption light of selected HBX derivatives were investigated (see Figure 3.10). The electron density lobe of hydroxyphenyl ring (yellow lobe) of HBI34 is larger than that of HBI14. Similarly, the electron density lobe of hydroxyphenyl ring of HBO34 and HBT34 are larger than those of HBO14 and HBT14, respectively. Comparison on the electron density of hydroxyl group (proton donor) and nitrogen heteroatom (proton acceptor) of selected HBX derivatives are discussed. The electron density lobe of hydroxyl group is smaller than those of nitrogen heteroatom. These results indicate that upon photoexcitation the acidity of proton donor and basicity of proton acceptor are increased in S_1, in which the K^* form is more stable than the E^* form leading to the favorable ESIPT process.

Table 3.3 Calculated maximum wavelengths of absorption spectra of enol form (nm), excitation energies (eV), oscillator strengths (*f*) and major contributions (%) of HBX and derivatives. The calculations were performed using TD-B3LYP/6-311+G(d,p) level.

Code	λ_{max}				Code	λ_{max}				Code	λ_{max}			
	nm	eV	*f*	MOs (%)		nm	eV	*f*	MOs (%)		nm	eV	*f*	MOs (%)
HBI	316	3.92	0.665	H→L (95%)	**HBO**	318	3.90	0.590	H→L (95%)	**HBT**	334	3.71	0.534	H→L (96%)
HBI1	326	3.80	0.627	H→L (96%)	**HBO1**	326	3.80	0.607	H→L (96%)	**HBT1**	344	3.60	0.479	H→L (97%)
HBI2	315	3.94	0.499	H→L (94%)	**HBO2**	320	3.88	0.432	H→L (95%)	**HBT2**	335	3.70	0.423	H→L (96%)
HBI3	317	3.91	0.465	H→L (96%)	**HBO3**	324	3.83	0.368	H→L (96%)	**HBT3**	343	3.62	0.372	H→L (97%)
HBI4	325	3.82	0.606	H→L (96%)	**HBO4**	327	3.79	0.502	H→L (95%)	**HBT4**	342	3.63	0.476	H→L (96%)
HBI12	335	3.70	0.351	H→L (97%)	**HBO12**	340	3.65	0.289	H→L (97%)	**HBT12**	350	3.54	0.310	H→L (97%)
HBI13	332	3.73	0.407	H→L (97%)	**HBO13**	340	3.65	0.313	H→L (97%)	**HBT13**	357	3.47	0.337	H→L (97%)
HBI14	348	3.56	0.488	H→L (97%)	**HBO14**	351	3.53	0.389	H→L (97%)	**HBT14**	362	3.43	0.401	H→L (97%)
HBI23	322	3.85	0.377	H→L (96%)	**HBO23**	332	3.73	0.303	H→L (97%)	**HBT23**	351	3.53	0.309	H→L (97%)
HBI24	328	3.78	0.423	H→L (96%)	**HBO24**	333	3.72	0.353	H→L (96%)	**HBT24**	345	3.59	0.362	H→L (97%)
HBI34	341	3.64	0.354	H→L (97%)	**HBO34**	349	3.55	0.286	H→L (97%)	**HBT34**	363	3.42	0.303	H→L (97%)

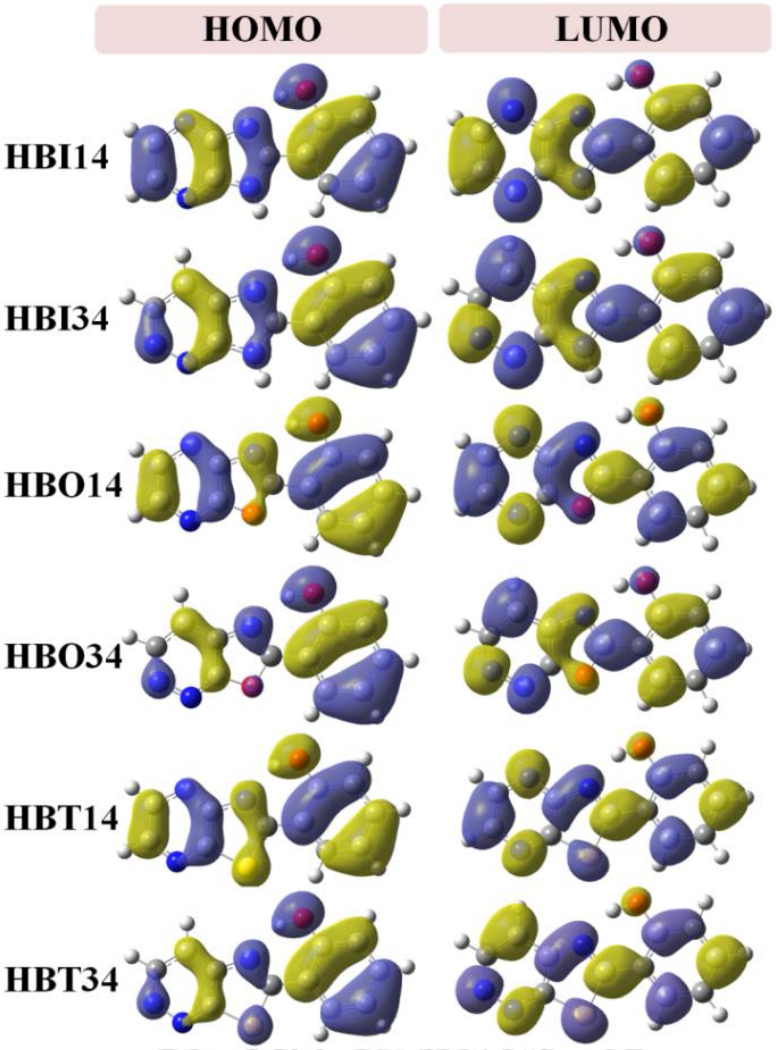

Figure 3.6 Frontier molecular orbitals of selected derivatives of HBX computed at B3LYP/6-311+G(d,p) level.

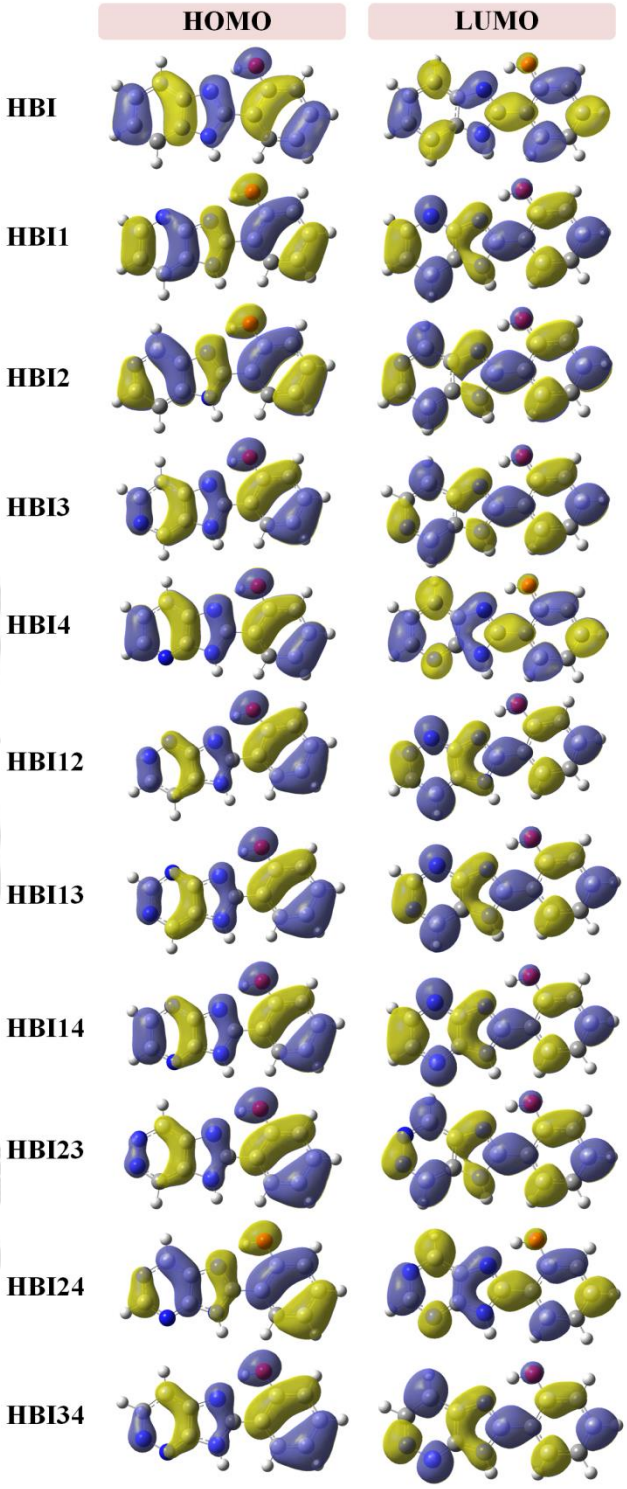

Figure 3.7 Frontier molecular orbitals of enol HBI and its derivatives computed at B3LYP/6-311+G(d,p) level.

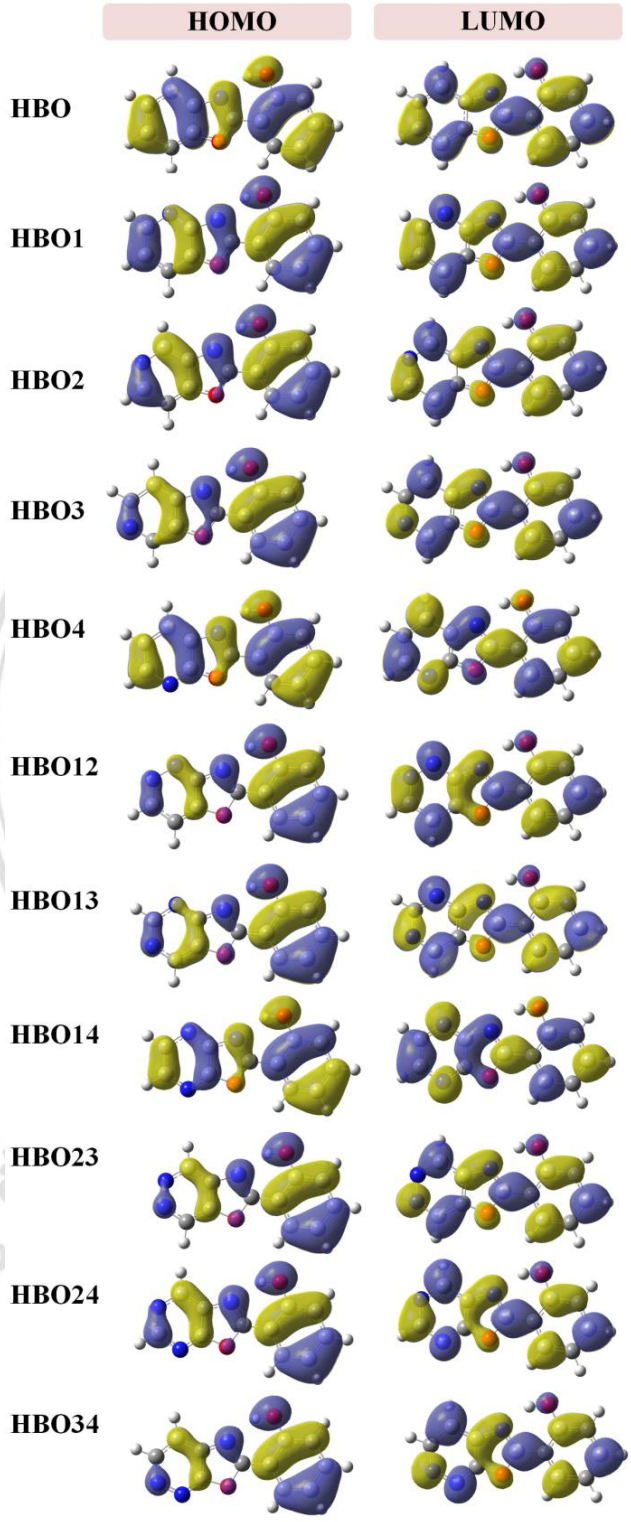

Figure 3.8 Frontier molecular orbitals of enol HBO and its derivatives computed at B3LYP/6-311+G(d,p) level.

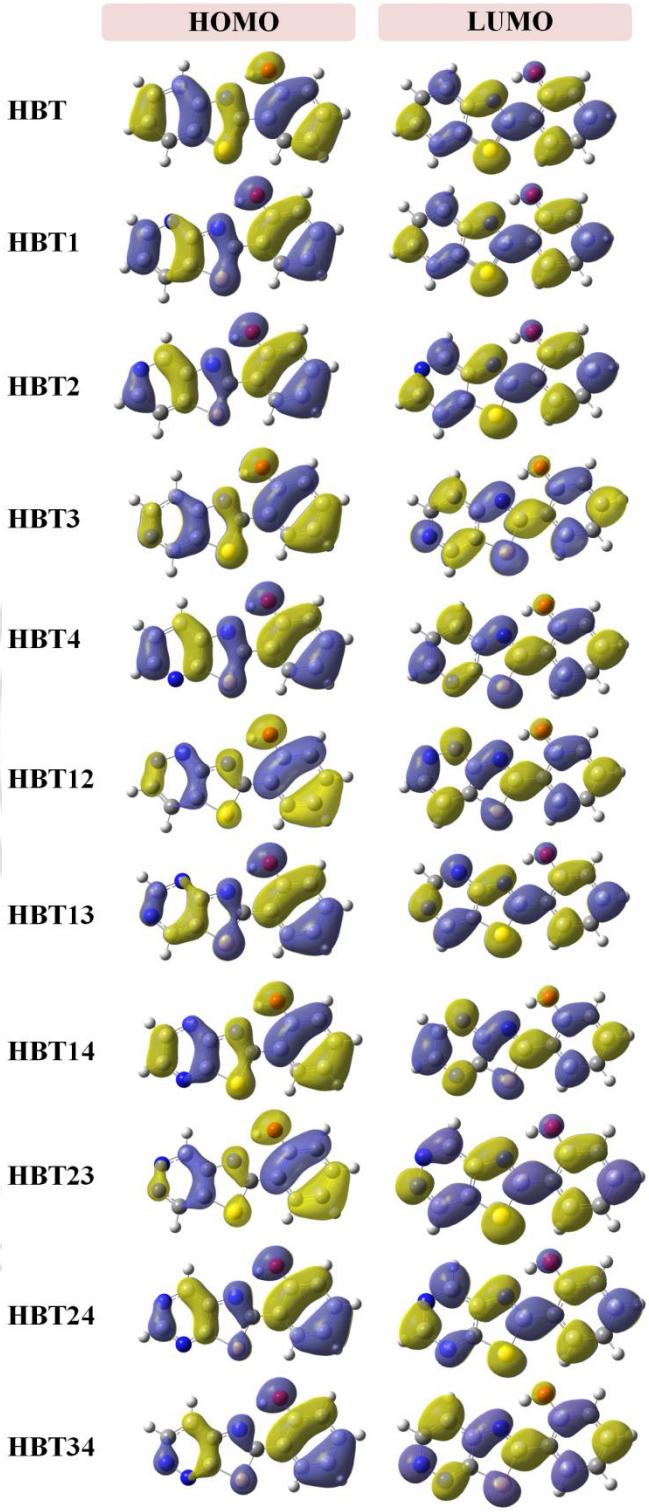

Figure 3.9 Frontier molecular orbitals of enol HBT and its derivatives computed at B3LYP/6-311+G(d,p) level.

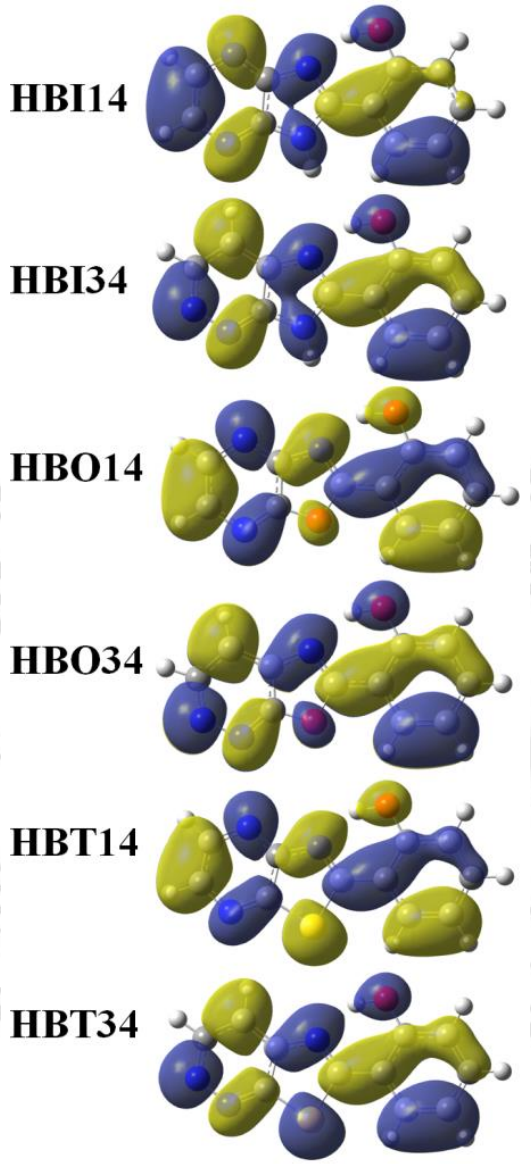

Figure 3.10 Density difference plot for selected derivatives of HBX computed at B3LYP/6-311+G(d,p) level. (isovalue = 0.0200 a.u.)

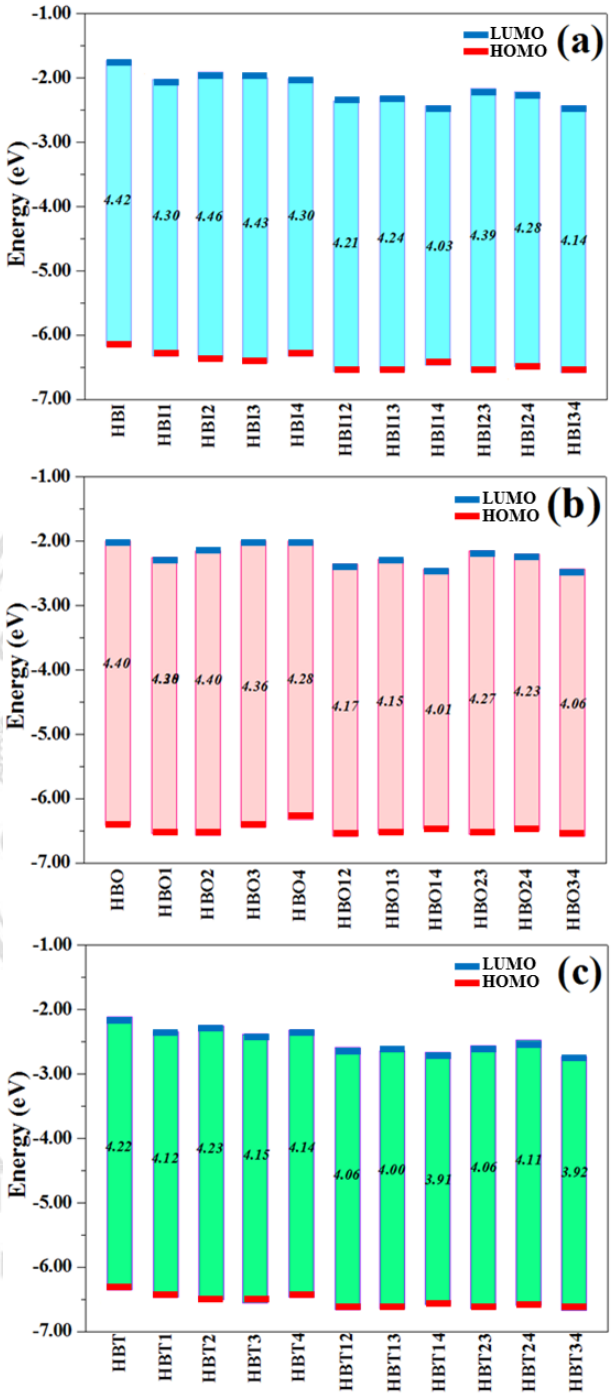

Figure 3.11 Diagram of calculated HOMO and LUMO energy levels and HOMO-LUMO gaps (eV) at B3LYP/6-311+G(d,p) level of enol absorption of (a) HBI, (b) HBO and (c) HBT and their derivatives.

3.3.5 Emission Spectra of Selected Derivatives

Investigation of Stokes shift of selected derivatives is discussed in this part. The calculated absorption spectra of enol form and calculated emission spectra of keto form for selected derivatives are shown in Figure 3.12. The λ_{max} of emission spectra of keto form for HBI14 and HBI34 are 512 and 497 nm, respectively (see Table 3.4). The λ_{max} of emission spectra of keto form for HBO14, HBO34, HBT14 and HBT34 are 520, 508, 515 and 516 nm, respectively. Therefore, nitrogen heteroatoms substituted at 1,4 and 3,4 positions of HBX strongly affect both absorption and emission spectra of HBX derivatives, causing a large Stokes shift. The larger Stokes shift can diminish self-absorption of fluorescent probes. Meanwhile, fluorescence emission in the longer wavelength region (low energy) can protect the tissue from photodamage and interfered by natural pigment in biological system [64, 150].

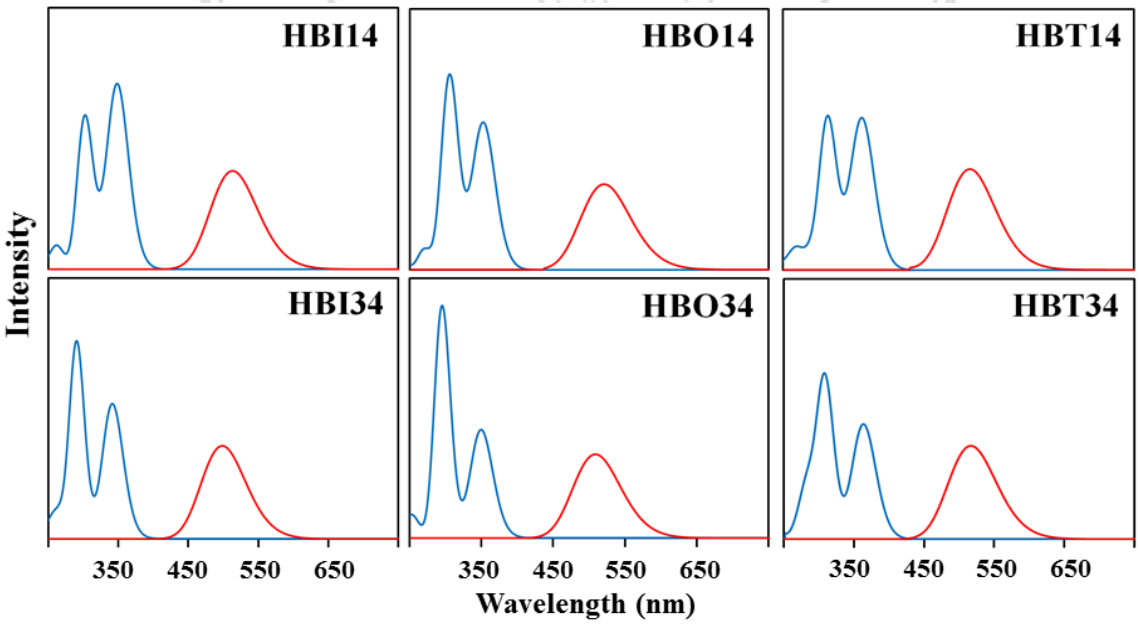

Figure 3.12 Calculated enol absorption (blue line) and keto emission (red line) spectra of selected HBX derivatives obtained from TD-B3LYP/6-311+G(d,p) level.

Table 3.4 Keto emission wavelengths (nm), excitation energy (eV), oscillator strength (*f*) and major contributions (%) for selected derivatives of HBI, HBO and HBT. The calculations were performed using TD-B3LYP/6-311+G(d,p) level.

Code	λ_1				λ_2			
	nm	**eV**	***f***	**MOs (%)**	**nm**	**eV**	***f***	**MOs (%)**
HBI14	512	2.42	0.260	H→L (100%)	321	3.97	0.454	H-2→L (94%)
HBI34	497	2.49	0.246	H→L (100%)	334	3.71	0.085	H→L+1 (97%)
HBO14	520	2.38	0.226	H→L (100%)	321	3.86	0.539	H-2→L (97%)
HBO34	508	2.44	0.223	H→L (100%)	345	3.59	0.047	H→L+1 (98%)
HBT14	515	2.40	0.267	H→L (100%)	333	3.72	0.533	H-2→L (97%)
HBT34	516	2.40	0.247	H→L (100%)	353	3.51	0.025	H→L+1 (99%)

3.3.6 Calculated IR Spectra of the Ground and Excited State of Selected Derivatives

The vibrational frequency of the O–H stretching mode can be used to support the strengthened of intramolecular hydrogen bond in the S_1 [21, 151]. The calculated infrared spectra of the O–H bonds in S_0 and S_1 of all selected HBX derivatives are shown in Figure 3.13 and the lengths of hydrogen bond (Å) of N–H and the distances of O–H in S_0 and S_1 calculated by B3LYP/6-311+G(d,p) level are listed in Table 3.5.

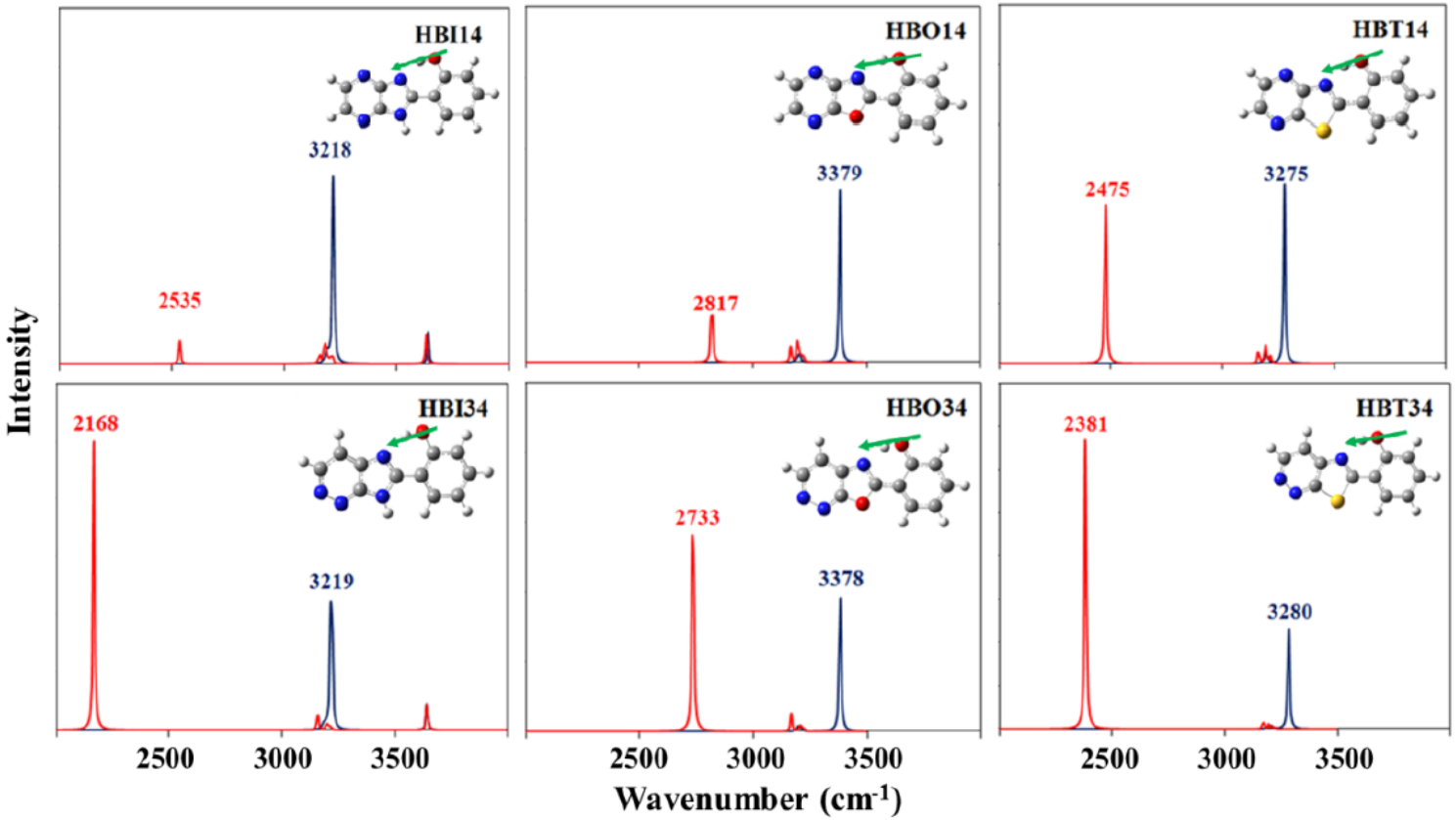

Figure 3.13 Calculated IR spectra of ground (blue line) and excited state (red line) of selected derivatives of HBI, HBO and HBT in the spectral region of O–H stretching mode calculated at the B3LYP/6-311+G(d,p) level.

Table 3.5 The lengths of hydrogen bond (Å) of N–H and O–H of HBX derivatives for ground and excited state optimized structures calculated by B3LYP/6-311+G(d,p) level of theory.

Code	Ground state		Excited state	
	N–H	O–H	N–H	O–H
HBI	1.70	0.99	1.67	1.00
HBI14	1.72	0.99	1.59	1.02
HBI34	1.72	0.99	1.52	1.05
HBO	1.78	0.98	1.73	0.99
HBO14	1.80	0.98	1.67	1.01
HBO34	1.79	0.98	1.65	1.01
HBT	1.73	0.99	1.65	1.01
HBT14	1.74	0.98	1.58	1.03
HBT34	1.74	0.98	1.56	1.03

For HBI derivatives, the calculated frequency of O–H stretching mode of HBI14 is located at 3218 cm^{-1} in the S_0, whereas this mode in the S_1 is 2535 cm^{-1}. For HBI34, this mode is located at 3219 cm^{-1}(S_0) and 2168 cm^{-1} (S_1). The strengthening of hydrogen bond in HBI14 is stronger than HBI34 (more red-shifted). For HBO derivatives, the O–H stretching modes at S_0 and S_1 for HBO14 and HBO34 show red shift from 3379 to 2817 cm^{-1} and from 3378 to 2733 cm^{-1}, respectively. Similarly, for HBT derivatives the O–H stretching mode of HBT14 is red shifted from 3275 cm^{-1} in S_0 to 2475 cm^{-1} in S_1. The O–H stretching mode of HBT34 is red shifted from 3280 cm^{-1} in S_0 to 2381 cm^{-1} in S_1. It can be clearly seen that the strengthening of hydrogen bond (red-shifted) is found in all selected HBX derivatives. This supports the enhanced probability of ESIPT, and also implies that the chances of open forms (where two rings stay out of plane) are rare.

By comparison of the red shift of O–H stretching mode of all HBX derivative, the values for HBI34, HBO34, and HBT34 are 1051, 645 and 899 cm^{-1}, respectively, which are larger than those of HBI14 (683 cm^{-1}), HBO14 (562 cm^{-1}) and HBT14 (800 cm^{-1}). It is noticed that the O–H hydrogen bond of HBX34 are weaker than those of HBX14

because the influence of substituted nitrogen heteroatom at 3,4 positions weakens the O–H bond (longer) in HBX derivatives, resulting in strengthen the N–H hydrogen bond (shorter). Thus, the ESIPT is most likely to occur in HBX34 than HBX 14 derivatives. These findings will be further supported by PECs and discussed in the next section.

3.3.7 Potential Energy Curves of the Ground and Excited State

The chance of ESIPT was investigated by PECs of selected HBX derivatives. The proton transfer PECs of these molecules were scanned based on constrained optimizations in their corresponding electronic states at fixed O–H distance for a series of values as reported in previous study[64, 148, 152]. The PECs were constructed, keeping the O–H bond distance fixed at the values in the range from 1.0 Å to 2.0 Å in step of 0.1 Å, as shown in Figure 3.14. The potential barrier of PECs in S_0 of HBI, HBO and HBT are 6.53, 9.82 and 7.80 kcal/mol, respectively. While, the potential barrier of in S_1 of HBI, HBO and HBT are 2.16, 3.61 and 1.42 kcal/mol, respectively. Therefore, the ESIPT are most likely to proceed in S_1 than S_0. For parent HBX molecules, the chance of ESIPT is found in this order: HBT > HBI > HBO.

The PECs of selected HBX derivatives compared to those of HBX parent molecules are discussed here. The PECs in S_1 of HBI14 and HBI34 exhibit a low barrier of 0.48 and 0.06 kcal/mol, respectively. In addition, the potential barriers in S_1 of HBO14, HBO34, HBT14 and HBT34 are 1.94, 1.42, 0.58 and 0.49 kcal/mol, respectively. The results of PECs of selected HBX derivatives indicates that the chances of ESIPT process of selected HBX derivatives are most likely to occur better than those of HBX parent molecules, due to the much lower barriers when compared with each HBX system.

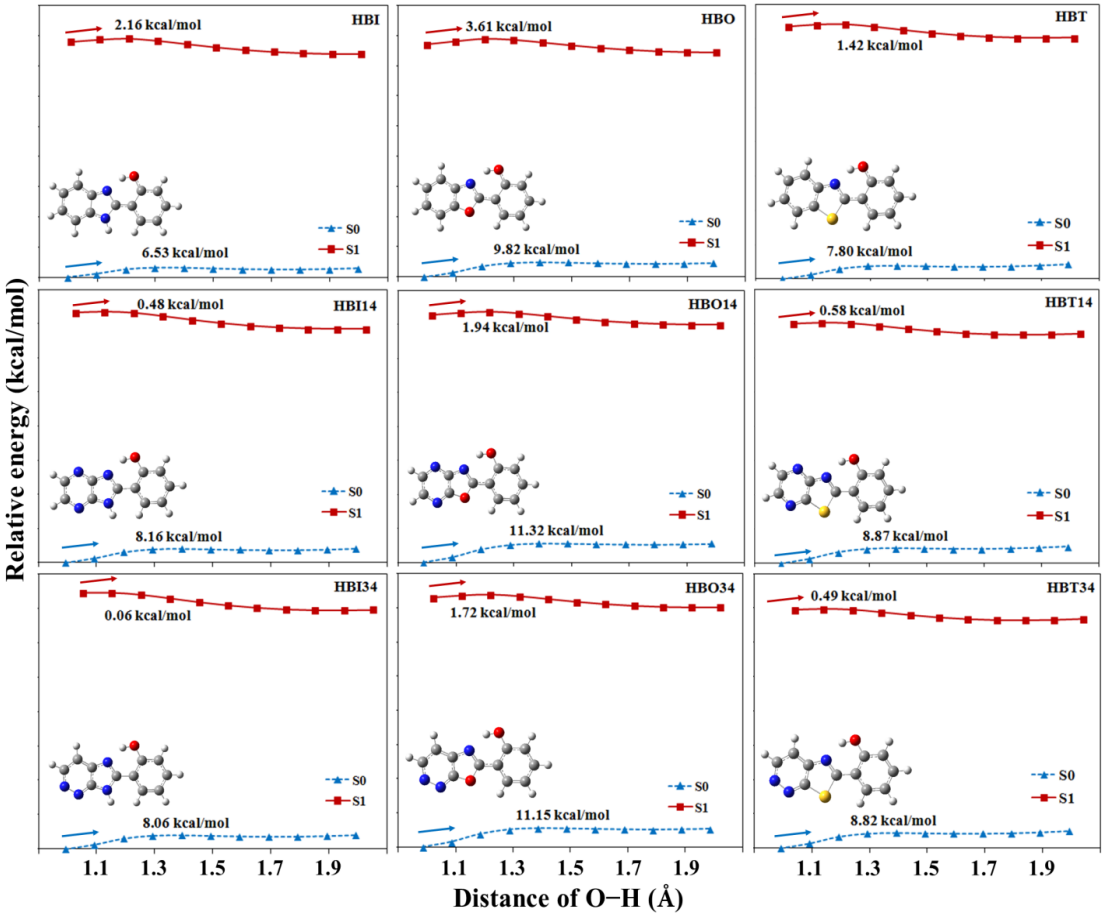

Figure 3.14 Potential energy curves of ground and excited states for selected derivatives of HBX and their derivatives with O–H bond length. The insert shows the corresponding optimized geometries.

3.4 Chapter Summary

This study has shown the effect of hetero nitrogen inserted in the benzene ring of benzimidazole (HBI), benzoxazole (HBO) and benzothaizole (HBT) moieties of HBX derivatives on the ESIPT process. Calculated spectra of HBI derivatives were systematically investigated by the method of choice at TD-DFT/TD-B3LYP/6-311+G(d,p) level, which was validated by a good agreement of calculated maximum wavelengths of HBI with the available experimental data. Adding the hetero nitrogen in HBX derivatives does not affect the planarity of these derivatives but significantly affect their photophysical properties. The absorption spectra of hetero nitrogen disubstitution are more red shift than hetero nitrogen monosustitution, particularly, the

absorption spectra of 1,4- and 3,4-disubstitution of HBX derivatives exhibit more red shift than other positions because the lone pair electron in the substituted hetero nitrogen might stabilize the π-conjugated system of benzimidazole, benzoxazole and benzothaizole ring of HBX derivatives. Furthermore, the chance of ESIPT is found to be in the order of HBT > HBI > HBO. The selected derivatives substituted with hetero nitrogen at 1,4 and 3,4 position of HBX derivatives could facilitate ESIPT process due to the nitrogen substitution makes O–H bond of selected derivatives weaker (longer) than those of HBX and the N–H distance of selected derivatives become stronger (shorter) in the S_1. Therefore, the obtained information in this present study particularly on prediction of photophysical properties of new designed fluorescent dyes will be very useful as guidance for chemists who are interested in developing the novel and effective ESIPT fluorescent dyes.